Bioinspired assembly

DOI: 10.1002/smll.200700357

DNA-Regulated Micro- and Nanoparticle Assembly **

*Mathew M. Maye, Dmytro Nykypanchuk, Daniel van der Lelie, and Oleg Gang**

The controllable self-assembly of micro- and nano-objects via biorecognition is attracting great attention because of the many possibilities it offers for creating complex abiotic systems with molecular-level spatial precision and structural tunability. Success in this approach promises advances in the design of new magnetic and plasmonic metamaterials,[1] cell-targeted delivery systems,[2] and biomolecular sensing.[3] As major efforts have focused on devising approaches to utilize attractive interactions provided by biomolecules, only recently have theoretical studies on biological[4] and hybrid systems[5] begun to highlight the crucial role of repulsion in modulating the efficiency of recognition, assuring error-proof self-organization and assembly morphology control. Herein, we describe a novel approach using DNA as a platform to tailor interobject attraction and repulsion, thereby broadening its versatility as a structural element in synthetic mesosystems.[6] In this approach, we finely balanced the attractive forces generated by complementary DNA hybridization with steric repulsion provided by noncomplementary DNA, effectively controlling interparticle interactions. By extending this approach to both micro- and nanoscale DNA-capped particles, which possess qualitatively different ranges of interparticle interactions, the general applicability of this concept for the regulation of particle assembly is demonstrated.

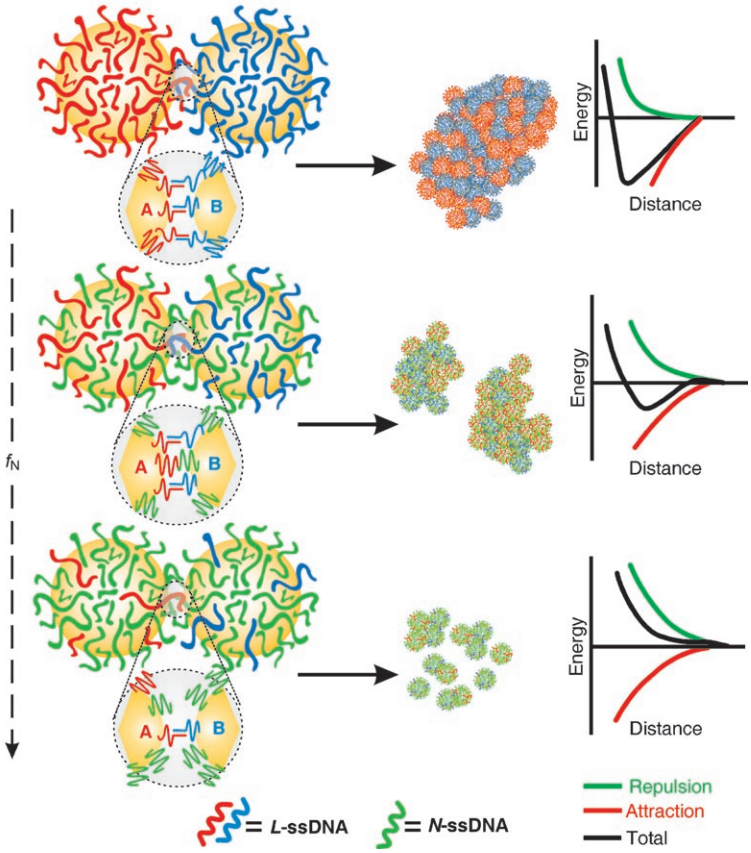

Scheme 1. An idealized scheme illustrating the assembly of DNA-capped particles with both *L* and *N* DNA capping. The set of energy diagrams illustrates the balance between attractive and repulsive forces depending on f_N.

Scheme 1 illustrates this approach, where single-stranded DNA (ssDNA) is utilized to regulate interparticle interactions over a wide size range and broad energy regime. Both DNA-capped microscale (1.9-μm-diamater polystyrene particles, PS) and nanoscale (9.6-nm-diameter gold particles, Au) systems consisted of an equimolar mixture of two types of particle (denoted as A and B), which were functionalized with a composition of complementary linker (*L*) ssDNA and noncomplementary (*N*) ssDNA. The surface fraction of *N* DNA, $f_N = [N]/([N]+[L])$, was controlled via functionalization conditions (see Supporting Information). The 30-base *L* DNA capping provided complementary recognition between particles via 15 base-pair (bp) duplex formation,

[*] Dr. M. M. Maye, Dr. D. Nykypanchuk, Dr. O. Gang
Center for Functional Nanomaterials
Brookhaven National Laboratory
Building 735, Upton, NY 11973 (USA)
Fax: (+1) 631-344-3093
E-mail: ogang@bnl.gov
Dr. D. van der Lelie
Biology Department
Brookhaven National Laboratory
Building 463, Upton, NY 11973 (USA)

[**] Research carried out at the Center for Functional Nanomaterials and the National Synchrotron Light Source at Brookhaven National Laboratory, was supported by the U.S. DOE, Office of Science and Office of Basic Energy Sciences, under contract No. DE-AC-02-98CH10866. M. M. M. acknowledges a Goldhaber Distinguished Fellowship at BNL sponsored by Brookhaven Science Associates. M. M. M. and D. N. contributed equally to this work.

Supporting information for this article is available on the WWW under http://www.small-journal.com or from the author.

while the N DNA capping provided steric repulsion of 30 noncomplementary bases. In the microscale PS system, this DNA capping provided only short-range interactions between particles A and B. In the nanoscale Au system, similar DNA capping was responsible for medium-range interactions. Despite the large difference in particle size, when the inter-particle distances are close to the DNA-capping thickness of $\approx$10 nm, L DNA hybridization is the major contribution to attraction, while the steric interactions of N ssDNA provide the basis for osmotic repulsion.

The microscale assembly of DNA-capped PS was monitored by optical microscopy. In this study, each PS contains $\approx$300000 total ssDNA strands, corresponding to an average surface coverage (σ_{PS}) of $\approx$0.3 strands per 10 nm^2. This abundance allows for hundreds of possible hybridized linkers between particles A and B.[7] Figure 1a shows a representative set of optical images of PS assembled for 24 h with f_N of i) 0.0, ii) 0.7, and iii) 0.9. The sizes of the aggregate show a clear tendency to decrease with increasing f_N. For example, at $f_N < 0.50$, only large aggregates, each containing thousands of particles, are observed with no evidence of nonassembled PS. At f_N between 0.50–0.90, the average size of the aggregates declines with increasing f_N so that samples at $f_N \approx 0.90$ contain only clusters of PS, and only isolated nonassembled PS particles were observed at $f_N \approx 0.95$. These results clearly demonstrate the strong influence of f_N on the average size of the assembled aggregates. This phenomenon cannot simply be explained by a reduced number of linkages between particles, since even a single hybridization provides a binding energy of $> 30\,kT$.[8] Thus, the effect of a reduction in aggregate size with increasing f_N points to the strong influence of osmotic repulsion, provided by the N ssDNA, in balancing the attractive interactions.[7]

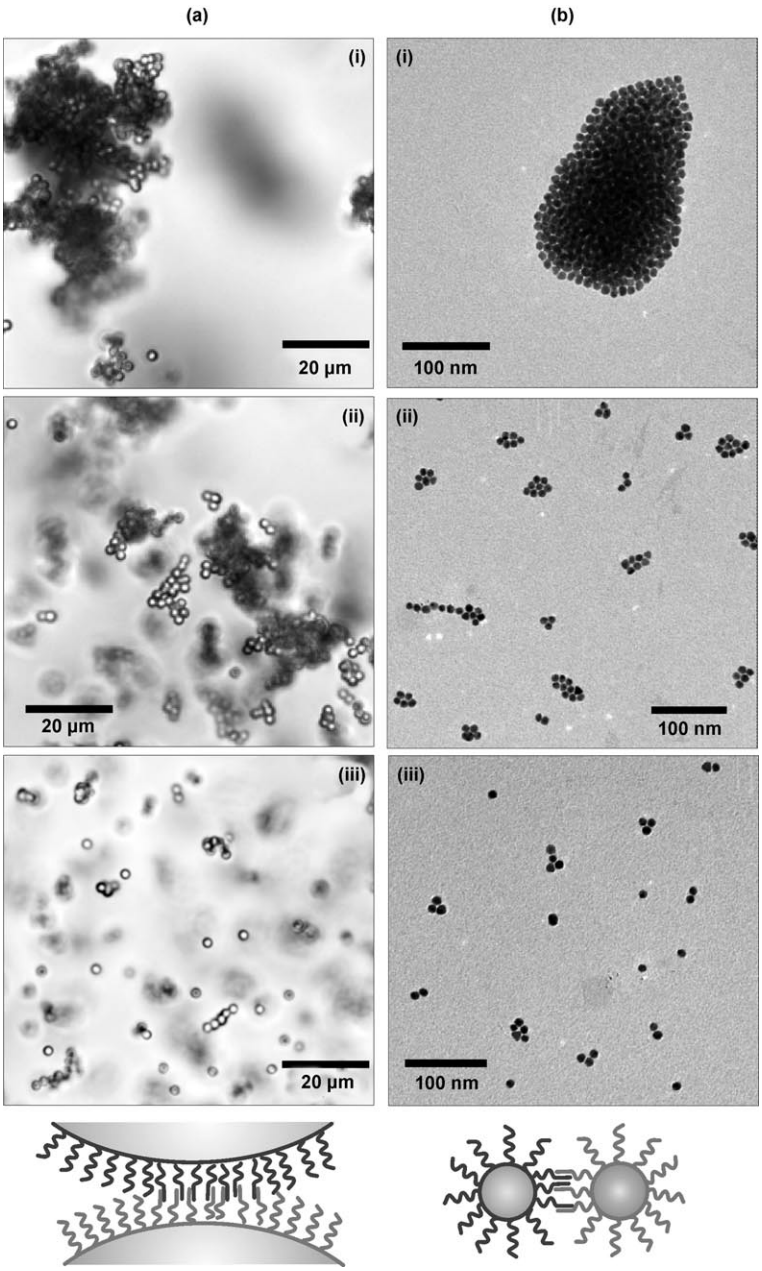

Figure 1. a) A set of optical images showing the aggregated 1.9-μm PS at f_N of i) 0.0, ii) 0.7, and iii) 0.9 ([A] = [B] = 0.05 % w/v, PBS buffer, pH 7.4). b) TEM images for aggregated 9.6-nm Au at f_N of i) 0.75, ii) 0.85, and iii) 0.95 ([A] = [B] = 7.5 nM, 10 mM phosphate buffer, 0.3 M NaCl, pH 7.1).

To investigate this effect in nanoscale systems, multiple aspects of the assembly of Au as a function of f_N were probed via transmission electron microscopy (TEM), UV/Vis spectroscopy, dynamic light scattering (DLS), and small-angle X-ray scatttering (SAXS). Each Au particle contained $\approx$60 total ssDNA, corresponding to a σ_{Au} of $\approx$1.9 DNA strands per 10 nm^2. In contrast to the microscale PS system, fewer than 10 potential linkers can be engaged in A–B hybridization, a feature that might significantly affect the aggregate structure when $f_N > \approx 0.8$, where the nominal number of linkages per particle is less than that required for close packing ($z = 12$). Figure 1b shows a set of TEM images for the assembled Au aggregates at f_N of i) 0.75, ii) 0.85, and iii) 0.95 after assembly for 4 h. Compared to the

micrometer-sized aggregates at $f_N < 0.50$ (see Supporting Information), we noted a dramatic drop in the size of the aggregates at f_N 0.75 to 100–200 nm. At f_N 0.85, small aggregates were formed, each containing 5–30 Au particles apiece, and at f_N 0.95 only small clusters were visible, as well as nonassembled Au. Similar aggregate sizes and morphology were observed after longer assembly times (>24 h). These TEM results reveal that the behavior of the Au nanosystems closely resembles that of the PS microsystem, wherein the assembly of aggregates is effectively suppressed by an increase in f_N.

The nanosystems also afforded the ability to monitor aggregate growth in situ. Figure 2a shows the DLS-monitored kinetic profiles for the Au aggregation at f_N 0.05–0.95, and Figure 2b reveals the final aggregate size and distribution after 2 h. These DLS measurements provide intensity-weighted hydrodynamic diameter values, $<D_h>_I$, which best represent the largest aggregates in the population and serve as a convenient comparison of f_N-influenced aggregate growth, without making assumptions about fractal dimensionality d_f, or the aggregates' internal structure. A significant decrease in aggregate growth was observed with f_N increase. Micrometer-sized aggregates formed within minutes for f_N 0.05, and small clusters only slightly larger than individual particles, $<D_h^0>_I = 27.5$ nm, were detected at f_N 0.95. The final $<D_h>_I$ of ≈150 nm, ≈60 nm, and ≈35 nm for f_N of 0.75, 0.85, and 0.95, respectively, closely followed the trend observed by TEM.

In contrast with classical coagulation theory,[9] the complexity of heteroaggregation, as shown for numerous systems,[10] is related to the details of cluster–cluster interactions,[11] cluster composition,[10] and coagulation constant time evolution.[12] Hence, the precise description of such systems remains problematic. However, based on the dynamic-scaling argument,[13] the kinetic profiles (Figure 2a) can be approximated by the power form $<D_h>_I \approx (t/\tau)^{\gamma}$, where t is time, τ *is* the characteristic aggregation time ($<D_h>_I(\tau) \approx 1.4 <D_h^0>_I$),[14] and γ relates to the homogeneity exponent $\lambda(\gamma = d_f(1-\lambda)^{-1})$ that parameterizes the characteristics of aggregation, from gelation to near-equilibrium clustering.[13,15] An increase in τ over multiple orders of magnitude is obtained from the kinetic profiles for f_N from 0.05 to 0.95. The particle-binding probability is approximately inversely proportional to τ, and decreases due to the interparticle potential change and geometrical constraints on hybridization at larger f_N.[7] For the predicted internal structures of aggregates, $d_f \approx 1.5$,[12] the obtained γ (Figure 2 caption) yields $0 < \lambda < 1$ at $f_N \leq 0.5$, and $\lambda < 0$ at $f_N \geq 0.75$. The negative value of λ implies that small-cluster formation is favored over large aggregates,[15] a finding that correlates with our observations. Similar behavior of finite-sized cluster formation was reported recently for a variety of systems, including polyelectrolytes and surfactants,[16] proteins,[17] and colloids,[18] which reflects the fine balance between repulsive and attractive interactions[18] in this system.

The rapid aggregation corresponding to low τ and positive λ values at $f_N \leq 0.50$ is indicative of predominantly attractive interaction between particles, as depicted in the energy profiles in Scheme 1. At intermediate concentrations of f_N 0.50–0.85, assembly attenuates, τ further increases, and λ decreases, asserting the presence of an increasing kinetic barrier (repulsion) and/or the reduction of attraction between particles. At f_N of 0.85–0.95, τ increases dramatically to 15 and 10^5, respectively, and λ becomes negative, suggesting that a near equilibrium exists between free particles and small clusters, or that there is a large energy barrier prohibiting assembly. To directly probe the effect of these interactions on the microscopic interparticle structure, we conducted in situ SAXS measurements on the aggregates (Figure 2c).[19] At $f_N \leq 0.5$, a near-constant spacing, d, of ≈17.3 nm was measured, while at f_N of 0.50–0.75 an increase to 18.6 nm was detected. This suggests that kinetic effects might be responsible for the slower assembly of aggregates at $f_N \leq 0.5$, while at higher f_N the influence of a stronger repul-

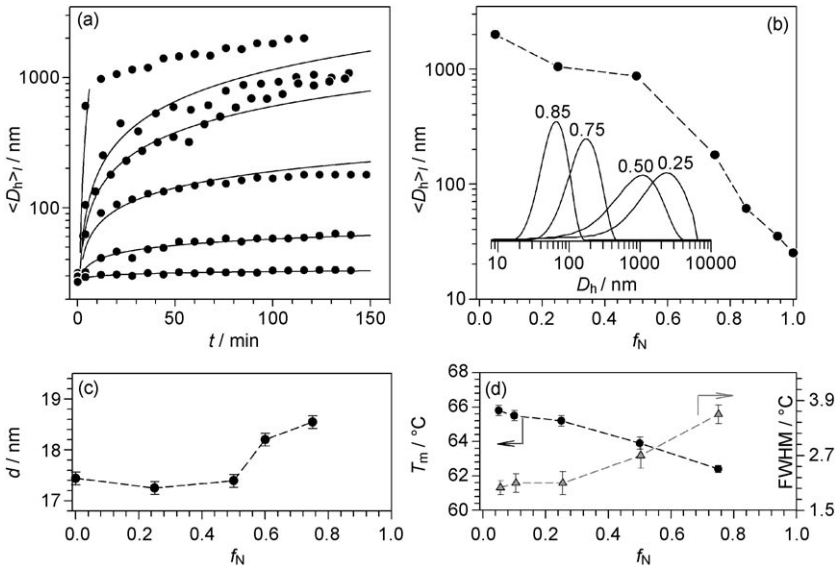

Figure 2. a) A set of DLS kinetic profiles for the assembly of Au at f_N values of 0.05, 0.25, 0.50, 0.75, 0.85, and 0.95 (from top to bottom). The solid lines represent a fit, as described in the text, with corresponding τ values of ~0.1, 0.8, 1.3, 1.5, 15, and 10^5 min, and γ values of 1.9, 0.73, 0.68, 0.37, 0.15, and 0.036 ([A] = [B] = 7.5 nM, 10 mM phosphate buffer, 0.3 M NaCl, pH 7.1). The limitations of DLS restrain the fits to aggregates of <1000 nm. b) A plot of aggregate hydrodynamic diameter $<D_h>_I$ after ~2 h assembly versus f_N as measured by DLS. The inset shows the final size distribution of the aggregates. c) A plot of spacing, d, related to the closest center-to-center distance between particles, as measured by in situ SAXS, versus f_N. d) A plot of T_m and full width at half-maximum (FWHM) of aggregate melting transition measured by UV/Vis spectroscopy (525 nm) versus f_N.

sion component in the interparticle potential results in greater d, which correlates with the observed suppression of aggregate size and assembly kinetics.

To further investigate this effect, the local interparticle DNA capping of the aggregates was probed thermodynamically by measuring their respective melting temperatures (T_m). The T_m of DNA-linked particle aggregates is related to the cooperativity of hybridization, which is affected by the number of linkages between particles,[20,21] their local density,[22] and the structure[23] of DNA. Figure 2d summarizes the relationship between T_m and f_N in the Au nanosystems, wherein we measured a progressive decrease in T_m from $\approx$66 to $\approx$62 °C between f_N of 0.05 and 0.75. This decrease in T_m was accompanied by a broadening in the melting transition, suggesting a decline in the number of linker hybridizations between particles, as well as in their local density.[21,22] Modeling this melting behavior (see Supporting Information) revealed a decrease in total melting-enthalpy change (ΔH_{TOT}) from $\approx$2725 to $\approx$961 kJ mol^{-1} when f_N varies from $f_{N1}=0.05$ to $f_{N2}=0.75$. This nearly threefold decrease in ΔH_{TOT} is in reasonable agreement with our estimate of the nominal reduction of the number of linkages between particles within the aggregates, $(1-f_{N1})/(1-f_{N2}) \approx 3.8$.

The intriguing result that both the PS and Au systems reveal similar f_N-dependent aggregation behavior, despite two orders of magnitude difference in particle size and a $\approx$sixfold difference in the average surface coverage can be understood based on the scaling of attractive and repulsive interparticle interactions with σ and surface curvature R^{-1}. Generally, at low σ when the DNA-capping structure does not change with particle size, both the attraction and repulsion energies scale with size as $\approx R$ (see Supporting Information). This results in a size-independent relationship but an overall lower magnitude of interactions energies for smaller particles. Changes in the structure of the ssDNA layer due to the rise in σ entails a $\approx 1.4\times$ increase in the capping thickness that scales as $\sigma^{1/5}$ for spherical surfaces,[24,25] with a corresponding enhancement of repulsion. In comparison, for rigid double-stranded (ds)DNA linkages, the entropic chain interactions are weak and the effect of an increased σ on attraction can be neglected. Conversely, at these σ, the two orders of magnitude increase in particle curvature, from 1/1000 nm^{-1} to 1/10 nm^{-1}, reduces entropic interDNA interactions, causing a decrease in DNA-capping thickness by $\approx$30%,[24,26] thus generating weaker repulsive interactions, in both range and magnitude. Thus, the nanosystem's increased σ is effectively counterbalanced by the increase in particle curvature, resulting in a similar f_N value ($\approx$0.95) at which the crossover to domination of repulsion occurs.

In summary, the ability to regulate the assembly of DNA-capped micro- and nanoparticles via balanced interparticle interactions over a broad range of particle sizes and interparticle interaction energies was demonstrated. The use of nonhybridizing DNA as a tool for steric repulsion allows for the control over a large range of interaction energies. While in the present form this DNA acts as a steric component, its high addressability can be easily exploited for future interaction fine tuning via DNA-designed recognition, or used as additional sites for more complex multicomponent or multiscale assembly systems.

Experimental Section

Polystyrene colloidal spheres (1.9 μm, Invitrogen Co.), with carboxylated surfaces were grafted with single-stranded 3′-primary-amine-modified ssDNA (Invitrogen Co.). The surface f_N was controlled by manipulating the ratio of L ssDNA, (L_A = 5′-TAC TTC CAA TCC AAT TTT TTT TTT TTT TTT-C_6H_{12}-NH_2-3′, L_B = 5′-ATT GGA TTG GAA GTA TTT TTT TTT TTT TTT-C_6H_{12}-NH_2-3′) and N ssDNA, (N = 5′-TTC TCT ACA CTC TCT TTT TTT TTT TTT TTT-C_6H_{12}-NH_2-3′) following procedures outlined in the Supporting Information. Assembly was carried out by mixing equimolar amounts of type A and type B particles to a final concentration of 0.1% w/v in phosphate buffered saline (PBS), pH 7.4, and incubating the mixture for 24 h on a rotating mixer at 4 °C.

Gold nanoparticles (9.6 ± 0.8 nm, Au) were synthesized following recent protocols[19] and then modified with 3′ thiol-functionalized ssDNA (IDT Inc.) following methods for high ssDNA coverage developed by Mirkin and co-workers.[21,22] The surface f_N was controlled by manipulating the L ssDNA, (L_A = 5-TAC TTC CAA TCC AAT GAT AGG TCG GTT GCT-C_3H_6-SH-3′, L_B = 5′-ATT GGA TTG GAA GTA GAT AGG TCG GTT GCT-C_3H_6-SH-3′) and N ssDNA, (N = 5′-TTC TCT ACA CTC TCT TTT TTT TTT TTT TTT-C_3H_6-SH-3′) concentrations during functionalization, as outlined in the Supporting Information. Assembly was carried out by combining equimolar amounts (7.5 nM) of type A and type B Au in a solution of 10 mM phosphate buffer, 0.2–0.3 M NaCl and pH 7.1.

Keywords:
colloids · DNA · interparticle interactions · nanoparticles · self-assembly

[1] J. Lee, P. Hernandez, J. Lee, A. O. Govorov, N. A. Kotov, *Nat. Mater.* **2007**, *6*, 291–295.
[2] a) Y. Choi, T. Thomas, A. Kotlyar, M. T. Islam, J. R. Baker, *Chem. Biol.* **2005**, *12*, 35–43; b) N. L. Rosi, D. A. Giljohann, C. S. Thaxton, A. K. R. Lytton-Jean, M. S. Han, C. A. Mirkin, *Science* **2006**, *312*, 1027–1030.
[3] N. L. Rosi, C. A. Mirkin, *Chem. Rev.* **2005**, *105*, 1547–1562.
[4] E. Shakhnovich, *Chem. Rev.* **2006**, *106*, 1559–1588.
[5] a) M. R. D'Orsogna, Y. L. Chuang, A. L. Bertozzi, L. S. Chayes, *Phys. Rev. Lett.* **2006**, *96*, 104302; b) N. A. Licata, A. V. Tkachenko, *Phys. Rev. E* **2006**, *74*, 041406; c) A. V. Tkachenko, *Phys. Rev. Lett.* **2002**, *89*, 148303.
[6] a) P. L. Biancaniello, A. J. Kim, J. C. Crocker, *Phys. Rev. Lett.* **2005**, *94*, 058302; b) J. D. Le, Y. Pinto, N. C. Seeman, K. Musier-Forsyth, T. A. Taton, R. A. Kiehl, *Nano Lett.* **2004**, *4*, 2343–2347; c) M. P. Valignat, O. Theodoly, J. C. Crocker, W. B. Russel, P. M. Chaikin, *Proc. Natl. Acad. Sci. USA* **2005**, *102*, 4225–4229; d) J. P. Zhang, Y. Liu, Y. G. Ke, H. Yan, *Nano Lett.* **2006**, *6*, 248–251.
[7] D. Nykypanchuk, M. M. Maye, D. van der Lelie, O. Gang, *Langmuir* **2007**, *23*, 6305–6314.
[8] J. SantaLucia, *Proc. Natl. Acad. Sci. USA* **1998**, *95*, 1460–1465.

[9] M. von Smoluchowski, *Z. Phys. Chem. (Leipzig)* **1917**, *92*, 124 – 168.
[10] J. M. Lopez-Lopez, A. Schmitt, A. Moncho-Jorda, R. Hidalgo-Alvarez, *Soft Matter* **2006**, *2*, 1025 – 1042.
[11] S. Bastea, *Phys. Rev. Lett.* **2006**, *96*, 028305.
[12] F. Pierce, C. M. Sorensen, A. Chakrabarti, *Langmuir* **2005**, *21*, 8992 – 8999.
[13] P. G. J. van Dongen, M. H. Ernst, *Phys. Rev. Lett.* **1985**, *54*, 1396 – 1399.
[14] H. Holthoff, M. Borkovec, P. Schurtenberger, *Phys. Rev. E* **1997**, *56*, 6945 – 6953.
[15] M. Tirado-Miranda, A. Schmitt, J. Callejas-Fernandez, A. Fernandez-Barbero, *Eur. Biophys. J.* **2003**, *32*, 128 – 136.
[16] S. Guillot, M. Delsanti, S. Desert, D. Langevin, *Langmuir* **2003**, *19*, 230 – 237.
[17] R. Piazza, *Curr. Opin. Colloid Interface Sci.* **2000**, *5*, 38 – 43.
[18] A. Stradner, H. Sedgwick, F. Cardinaux, W. C. K. Poon, S. U. Egelhaaf, P. Schurtenberger, *Nature* **2004**, *432*, 492 – 495.
[19] M. M. Maye, D. Nykypanchuk, D. van der Lelie, O. Gang, *J. Am. Chem. Soc.* **2006**, *128*, 14020 – 14021.
[20] a) D. B. Lukatsky, D. Frenkel, *Phys. Rev. Lett.* **2004**, *92*, 068302.
[21] J. J. Storhoff, A. A. Lazarides, R. C. Mucic, C. A. Mirkin, R. L. Letsinger, G. C. Schatz, *J. Am. Chem. Soc.* **2000**, *122*, 4640 – 4650.
[22] a) R. C. Jin, G. S. Wu, Z. Li, C. A. Mirkin, G. C. Schatz, *J. Am. Chem. Soc.* **2003**, *125*, 1643 – 1654; b) A. K. R. Lytton-Jean, C. A. Mirkin, *J. Am. Chem. Soc.* **2005**, *127*, 12754 – 12755; c) J. Xu, S. L. Craig, *J. Am. Chem. Soc.* **2005**, *127*, 13227 – 13231.
[23] N. C. Harris, C. H. Kiang, *Phys. Rev. Lett.* **2005**, *95*, 046101.
[24] N. Dan, M. Tirrell, *Macromolecules* **1992**, *25*, 2890 – 2895.
[25] M. Daoud, J. P. Cotton, *J. Phys.* **1982**, *43*, 531 – 538.
[26] S. T. Milner, T. A. Witten, *J. Phys.* **1988**, *49*, 1951 – 1962.

Received: May 22, 2007
Published online on September 11, 2007

